Letter

Band-selective third-harmonic generation in superconducting MgB_2: Possible evidence for the Higgs amplitude mode in the dirty limit

Sergey Kovalev,[1] Tao Dong,[2,3,*] Li-Yu Shi,[3] Chris Reinhoffer,[4] Tie-Quan Xu,[5] Hong-Zhang Wang,[5] Yue Wang,[5] Zi-Zhao Gan,[5] Semyon Germanskiy,[4] Jan-Christoph Deinert,[1] Igor Ilyakov,[1] Paul H. M. van Loosdrecht,[4] Dong Wu,[3] Nan-Lin Wang,[3,6] Jure Demsar,[2] and Zhe Wang[7,4,1,†]

[1]*Institute of Radiation Physics, Helmholtz-Zentrum Dresden-Rossendorf, 01328 Dresden, Germany*
[2]*Institute of Physics, Johannes Gutenberg-University Mainz, 55128 Mainz, Germany*
[3]*International Center for Quantum Materials, School of Physics, Peking University, Beijing 100871, China*
[4]*Institute of Physics II, University of Cologne, 50937 Cologne, Germany*
[5]*Applied Superconductivity Center and State Key Laboratory for Mesoscopic Physics, School of Physics, Peking University, Beijing 100871, China*
[6]*Beijing Academy of Quantum Information Sciences, Beijing 100913, China*
[7]*Fakultät Physik, Technische Universität Dortmund, 44221 Dortmund, Germany*

(Received 15 May 2020; revised 7 October 2020; accepted 13 October 2021; published 27 October 2021)

We report on time-resolved linear and nonlinear terahertz spectroscopy of the two-band superconductor MgB_2 with a superconducting transition temperature $T_c \approx 36$ K. Third-harmonic generation (THG) is observed below T_c by driving the system with intense narrow-band THz pulses. For the pump-pulse frequencies $f = 0.3$, 0.4, and 0.5 THz, the temperature-dependent evolution of the THG signals exhibits a resonance maximum at the temperatures with the resonance conditions $2f = 2\Delta_\pi(T)$ fulfilled, for the dirty-limit superconducting gap $2\Delta_\pi$. In contrast, for $f = 0.6$ and 0.7 THz with $2f > 2\Delta_\pi(T \to 0) = 1.03$ THz, the THG intensity increases monotonically with decreasing temperature. Moreover, for $2f < 2\Delta_\pi(T \to 0)$ the THG is found nearly isotropic with respect to the pump-pulse polarization. These results suggest a predominant contribution of the driven Higgs amplitude mode of the dirty-limit π-band superconducting gap, pointing to the importance of scattering for observation of the Higgs mode in superconductors.

DOI: 10.1103/PhysRevB.104.L140505

Novel quantum phenomena, which may not be accessible to the linear spectroscopy in equilibrium states, can often be visualized in driven nonequilibrium states. A prominent example is the Higgs amplitude mode in a superconductor [1–4]. With the $U(1)$ rotational symmetry spontaneously broken, a superconducting state is characterized by fluctuations of the amplitude and phase of the superconducting gap. The Higgs mode corresponding to the amplitude fluctuations is a scalar excitation without charge or electric/magnetic dipoles. As such, it cannot directly couple to external probes in the linear-response regime [4].

Terahertz (THz) harmonic generation has been suggested to be an efficient probe to reveal the Higgs mode in superconductors [5–11]. Here, an intense narrow-band THz pulse can drive a superconductor out of equilibrium, and trigger the coherent Higgs oscillations of the superconducting order parameter. The driven Higgs mode with twice the frequency of the pump pulse is further coupled to the pump pulse, leading to third-harmonic generation (THG) [4]. Experimentally it is, however, not straightforward to unambiguously attribute the THG signal to the driven Higgs mode. In addition to a major enhancement of the THG signal below the superconducting transition temperature T_c, the Higgs mode excitation should give rise to a peak in the THG signal when twice the pump-pulse frequency matches the superconducting gap frequency. Although these features were observed in the *s*-wave superconductor NbN [5], it was argued that the THG signal is more likely a result of charge density fluctuations due to THz driven Cooper-pair breaking [12]. The contribution of charge density fluctuations to THG is, however, not always dominant, as pointed out by further theoretical studies [11,13,14]. Especially when correlation effects and/or impurity scattering are pronounced, the contribution due to the driven Higgs mode will dominate the THG signal. Moreover, the two competing scenarios suggested different dependences on the polarization of the driving THz field with respect to the crystalline axis. NbN was found to exhibit an isotropic THG signal with respect to the polarization of the driving field, a signature supporting the assignment of the THG to the driven Higgs mode, whereas the THG from charge density fluctuations is expected to be anisotropic [7].

Recently, extensive theoretical studies of the THG in two-band superconductors addressed not only the Higgs amplitude fluctuations in individual bands, but also the so-called Leggett phase mode, resulting from the interband coupling [15–19]. Here, fluctuations of the relative phase between the two-coupled order parameters, the Leggett mode, are also charge neutral and do not linearly couple to the electromagnetic

*taodong@pku.edu.cn
†zhe.wang@tu-dortmund.de

field [15]. Similar to the Higgs modes, the Leggett mode with frequency ω_L can be resonantly excited by a multicycle THz pulse with frequency f satisfying the condition of $2f = \omega_L$, which is expected to be manifested by a resonance peak in the THG [16–19]. Moreover, paramagnetic impurity scattering has been predicted to play a decisive role in the nonlinear response of the superconductors [14,19–22]. While in the clean limit the THG was found to be dominated by pair breaking [12,17], the contribution of the Higgs mode can be significantly enhanced by impurity scattering. Thus, in the dirty limit, the Higgs amplitude fluctuations are more predominant than the charge density fluctuations, while the Leggett phase fluctuations in a two-band superconductor are much weaker and hardly detectable in a THG experiment [19].

Motivated by these theoretical advances, we performed THz spectroscopic measurements in the two-band superconductor MgB_2 in the linear- and nonlinear-response regimes. The linear response reveals the smaller gap $2\Delta_\pi$ to be in the dirty superconductor limit. In contrast, no spectroscopic signature is evident in the vicinity of the larger gap $2\Delta_\sigma$ in the accessible spectral range, suggesting it may be in the clean limit. THz third-harmonic generation is studied as a function of temperature for various driving frequencies and as a function of polarization with respect to the crystalline sample orientation. Temperature-dependent THG exhibits peaks at temperatures, where $2f$ matches $2\Delta_\pi$, whereas no anomalies are observed for $2f$ matching either the frequency of the larger gap or of the Leggett mode. These results point to a predominant contribution of the Higgs mode of the π band in the dirty limit.

High-quality single-crystalline MgB_2 thin films with the c-axis epitaxy were grown on a MgO (111) substrate by using a hybrid physical-chemical vapor deposition method, and characterized by x-ray diffraction and charge transport measurements [23–25]. Optical measurements were carried out on 13-nm-thick MgB_2 films grown on a 5×5 mm MgO substrate of 0.33 mm thickness, with $T_c \approx 36$ K [23,24]. Linear time-domain THz spectroscopy was performed using a GaAs photoconductive antenna as the THz source, driven by a Ti:sapphire oscillator generating 35 fs pulses at a 800 nm central frequency with a repetition rate of 80 MHz [26]. For the THG measurements, broadband THz pulses were generated via a tilted pulse-front scheme utilizing a $LiNbO_3$ crystal [27,28], driven by a Ti:sapphire amplifier generating 100 fs pulses at 800 nm with a pulse energy of 1.5 mJ and a repetition rate of 1 kHz. The spectral distribution of the generated THz pulses was optimized for around 0.7 THz central frequency. Narrow-band multicycle THz pulses were produced using bandpass filters with 20% bandwidth. The THz radiation was detected by electro-optic sampling at a ZnTe crystal. Temperature-dependent measurements were performed using helium-flow cryostats.

The two-band BCS-type superconductor MgB_2 crystallizes in a hexagonal structure with the space group $P6/mmm$ [see Fig. 1(a)] [29–34]. At 4.2 K two superconducting gaps of $2\Delta_\pi = 1.1$ and $2\Delta_\sigma = 3.6$ THz were found in the π and σ bands, respectively [31]. Figure 1(b) shows THz electric field transients transmitted through the MgB_2/MgO sample at 4 and 36 K, compared to that through the reference bare MgO substrate at 4 K. By Fourier transformation of the time-domain signals, one can obtain the transmission and phase shift in the frequency domain, from which complex optical conductivity is derived.

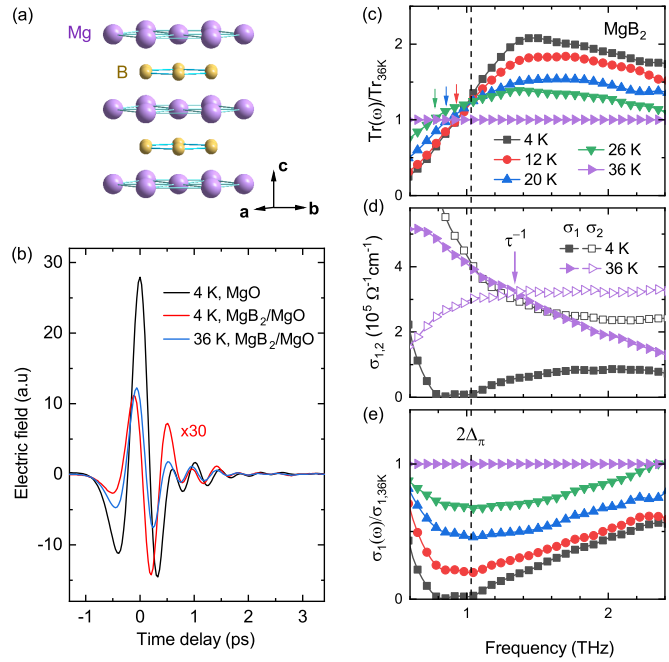

FIG. 1. (a) Layered crystallographic structure of MgB_2. THz electromagnetic waves propagated along the c axis. (b) Transmitted THz electric field as a function of time delay, for MgB_2/MgO at 4 and 36 K and for the bare MgO substrate at 4 K. The data for MgB_2/MgO at 4 and 36 K are magnified by a factor of 30 for clarity. (c) Ratio of transmission for various temperatures with respect to 36 K. The arrows indicate the frequencies at which the ratio curves cross unity. (d) Real σ_1 and imaginary σ_2 parts of optical conductivity at 36 and 4 K. The arrow indicates the crossing point of the σ_1 and σ_2 curves at $\tau^{-1} = 1.34$ THz for 36 K. (e) Ratio of σ_1 for various temperatures with respect to 36 K. The dashed line indicates the excitation gap $2\Delta_\pi = 1.03$ THz at 4 K.

The transmission ratio with respect to 36 K for various temperatures below T_c is shown in Fig. 1(c) as a function of frequency. For all the temperatures the transmission ratio increases first with decreasing frequency, and then drops continuously down to a value smaller than the unity. The curves of the different temperatures below T_c intersect with each other, forming an isosbestic point [35–37]. As indicated by the dashed line, the isosbestic point around 1.03 THz coincides with the onset of optical conductivity σ_1 at 4 K [see Fig. 1(d)], which reflects the formation of the superconducting gap in the π band, in agreement with the reported results [31–33,38].

Figure 1(d) shows the extracted complex optical conductivity in the normal state (36 K) and at 4 K, clearly demonstrating the opening of the gap below 36 K. In the normal state, the data are consistent with the free-carrier Drude response. The limited bandwidth prevents us from performing a detailed analysis using two Drude components with reliable accuracy. Instead we estimate the scattering rate within the simple Drude scenario as the crossing point between σ_1 and σ_2. The extracted value $\tau^{-1} = 1.34$ THz is indicated by the arrow

in Fig. 1(d). The estimated scattering rate in our sample is comparable to the values reported in Refs. [39,40], but considerably lower than the values of 4.5 and 9 THz respectively reported in Ref. [41] and Ref. [38].

In the superconducting state the spectral weight of σ_1 at the finite frequency is depleted due to the opening of the superconducting gap as shown in Figs. 1(d) and 1(e). At 4 K, σ_1 drops almost to zero below the superconducting gap at $2\Delta_\pi = 1.03$ THz ~ 4.26 meV, while σ_2 exhibits a $1/\omega$ behavior. We also note the upturn in σ_1 at frequencies below $\sim$0.7 THz, which is consistently observed in MgB_2 at low frequencies [38,41]. This could be caused by an additional absorption of unpaired carriers, which seems to be intrinsic in nature [41].

The observed superconducting gap and temperature dependence of the optical conductivity are comparable with that reported for thin-film samples in Refs. [38,41]. Quantitatively, the broadband normal state optical response was modeled also using two Drude terms, from which different scattering rates for the σ and π bands were derived [42,43]. Similar to the case in Refs. [39,40], our data suggest that $2\Delta_\pi < \tau^{-1} < 2\Delta_\sigma$. Note that the scattering rates extracted in the literature are generally higher in the π band than in the σ band [42,43]. Thus, our extracted value likely corresponds to the scattering rate of the σ band. This suggests that superconductivity can be considered to be in the dirty limit for the π band and in the clean limit for the σ band. The contrast between the two bands seems crucial for the understanding of the nonlinear response, as presented in the following.

Due to the low-frequency residual conductivity observed even at 4 K [Fig. 1(e)], the temperature dependence of the superconducting gap $2\Delta_\pi(T)$ cannot be straightforwardly derived, e.g., by fitting the frequency-dependent optical conductivity according to the Mattis-Bardeen theory [38]. To extract qualitatively the temperature dependence of the gap in the π band, we approximate $2\Delta_\pi(T)$ by the point where the normalized transmission crosses the unity. As indicated by the arrows in Fig. 1(c), the crossing point shifts continuously towards lower frequency with increasing temperature. By multiplying the extracted crossing point frequencies with the ratio of $2\Delta_\pi = 1.03$ THz and the crossing point frequency at 4 K, we obtain $2\Delta_\pi(T)$, as shown in Fig. 2(c) by the solid symbols. These results agree very well with the scanning tunneling spectroscopy data [31].

We observed third-harmonic radiation in MgB_2 by pumping the system with multicycle THz pulses. Figure 2(a) displays the time-domain wave form of the $f = 0.5$ THz pump pulse. Driven by this pulse, the generated radiation of the sample was recorded with or without a $3f = 1.5$ THz bandpass filter in the time domain [see Fig. 3(a) for an illustrative sketch of the experimental setup]. Figure 2(b) shows the spectrum of the generated radiation without a $3f$-bandpass filter obtained via Fourier transformation of the time-domain signal at 6 K.

The temperature dependence of the obtained THG signal with a $3f$-bandpass filter is presented in Fig. 2(d). Starting from 5 K, the observed THG intensity for $f = 0.5$ THz increases continuously with increasing temperature until about 19 K, which is followed by a continuous decrease at higher temperatures towards T_c. Above T_c, the THG signal is dramatically reduced. The enhancement of the third-harmonic generation below T_c clearly reflects the nonlinear response of the superconducting state. Moreover, the intensity maximum for $3f = 1.5$ THz occurs right at a temperature where the resonance condition $2f = 2\Delta_\pi$ is fulfilled, which is indicated by the vertical dashed line in Figs. 2(c) and 2(d). However, such resonant behavior is not observed in the vicinity of temperatures where the resonance condition would be fulfilled for the gap in the σ band, or for the Leggett mode that was previously determined from the Raman response [44–46], even though such resonance peaks were predicted in the clean limit [16,17]. Although the observed THG signal here is dominated by the response of the π band, one may still expect to reveal the Leggett mode and/or response of the σ band via complementary pump-probe approaches, such as a higher-frequency THz-pump broad-band THz probe [4,46]. A recent study shows that by using a pump pulse of 1.4 THz, which is evidently greater than the π gap $2\Delta_\pi = 1.03$ THz, it is possible to reveal the signature of the Leggett mode [46]. For such a high-frequency pump pulse, the response of the

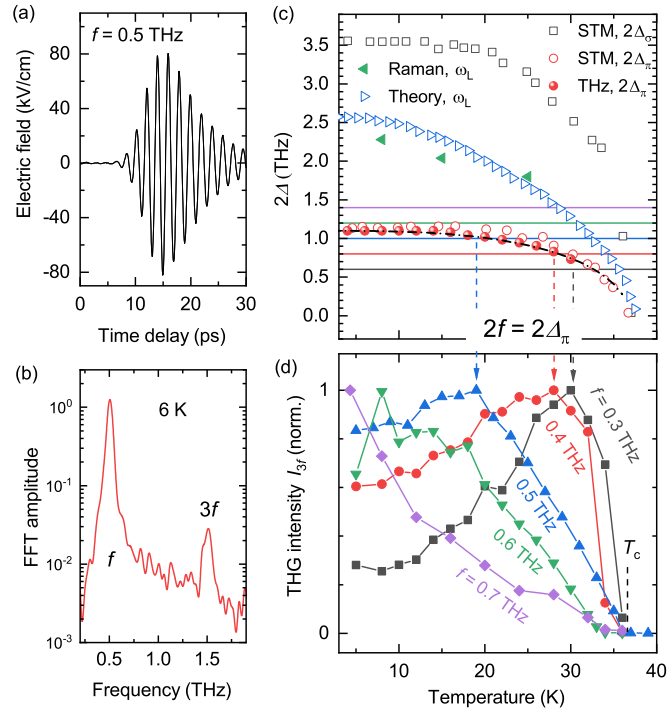

FIG. 2. (a) Electric field of the $f = 0.5$ THz pump pulse in the time domain. (b) Spectrum of the generated radiation from the sample at 6 K. (c) Temperature dependence of superconducting gaps as determined by scanning tunneling microscopy (STM) for the σ and π bands (squares and circles) [31], and as estimated from Fig. 1(c) (spheres). Leggett mode vs temperature as observed in Raman spectroscopy (left triangles) [44,45] and obtained from theoretical calculations (right triangles) [46]. The horizontal solid lines indicate $2f$ for $f = 0.3$, 0.4, 0.5, 0.6, and 0.7 THz, respectively. (d) The corresponding normalized THG intensity I_{3f} as a function of temperature, measured through two bandpass filters of $3f$. The vertical dashed lines indicate the peak positions in the temperature-dependent curves, where the corresponding resonance condition $2f = 2\Delta_\pi$ is fulfilled simultaneously.

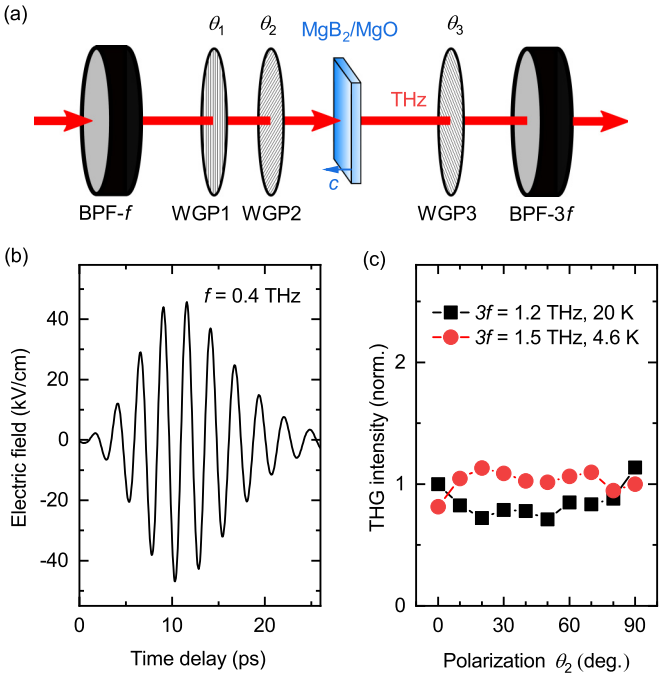

FIG. 3. (a) Schematic illustration of the setup for polarization-dependent THG measurements. The THz electromagnetic waves propagate along the sample c axis. BPF-f and BPF-3f denote bandpass filters for the fundamental frequency and the THG, respectively. WGP's denote wire-grid polarizers. (b) Wave form of the $f = 0.4$ THz pump pulse for the polarization-dependent measurements. (c) Normalized THG intensity as a function of the pump-pulse polarization, varied by tuning the angle θ_2 of WGP2, which is obtained for $f = 0.4$ and 0.5 THz at 20 and 4.6 K, respectively.

π band should be primarily due to pair-breaking excitations [see Fig. 1(e)].

To further study the temperature-dependent behavior, we performed THG measurements for lower and higher pump-pulse frequencies, i.e., $f = 0.3$, 0.4, 0.6, and 0.7 THz. As presented in Fig. 2(d), for $f = 0.3$ and 0.4 THz, i.e., $2f < 2\Delta_\pi(T \to 0)$, the temperature-dependent THG curves exhibit maxima at 30 and 28 K, respectively, matching the resonance condition $2f = 2\Delta_\pi$ (indicated by the arrows). In contrast, for $2f > 2\Delta_\pi(T \to 0)$, i.e., $f = 0.6$ and 0.7 THz, the THG signal decreases monotonically with increasing temperature, without exhibiting a peaklike enhancement. Although the σ band located in the clean limit is in general expected to exhibit a stronger THG signal due to the charge density fluctuations, for none of the five frequencies we resolved a maximum corresponding to the resonance condition of the σ band. These observations suggest that the observed THG signal is unlikely being dominated by the response from the σ band (e.g., charge density fluctuations or Higgs amplitude fluctuations). Thus, we tend to ascribe the observed THG signals for $2f < 2\Delta_\pi(T \to 0)$ to the Higgs amplitude fluctuations of the smaller π gap in the dirty limit, which is in line with recent theoretical results [14,19].

We further characterized the THG signal in the superconducting state as a function of pump-pulse polarization. As illustrated in Fig. 3(a), the polarization of the pump pulse is tuned by the wire-grid polarizer (WGP2) directly in front of the sample. To assure a constant pump fluence at the sample position, another WGP1 is placed between WGP2 and the bandpass filter (BPF-f) of the fundamental frequency. After the sample, an additional wire-grid polarizer (WGP3) is inserted with a fixed polarization direction at 45° with respect to the horizontal direction. With this polarizer, the electro-optic sampling at the ZnTe crystal (not shown) was optimized for detection. Before measuring the polarization dependence of the THG signals, the setup was calibrated by adjusting θ_1 while setting θ_2 for different polarizations, to ensure a constant pump fluence at the sample position.

Figure 3(b) shows the wave form of the pump pulse of $f = 0.4$ THz. The polarization-dependent THG intensity from the sample is presented in Fig. 3(c) for $3f = 1.2$ and 1.5 THz at 20 and 4.6 K, respectively. The peak fields of the corresponding pump pulses were set at 47 and 54 kV/cm for $f = 0.4$ and 0.5 THz, respectively. In the presented THG intensity, a factor $\cos^2(\theta_2 - \theta_3)$ due to the polarization difference between WGP2 and WGP3 has been taken into account. We can see that the THG intensity is only weakly dependent on the pump-pulse polarization for both the $f = 0.4$ and the 0.5 THz pump pulses. It is worth noting that a nearly polarization-independent THG is not necessarily the characteristic for the Higgs amplitude mode in general. On the one hand, isotropic THG was indeed theoretically predicted for the Higgs mode [7,11] and reported for the s-wave superconductor NbN [7]. On the other hand, for multiband or unconventional superconductors (e.g., $d + s$ wave), theoretical studies showed that the THG due to the Higgs mode can also be polarization dependent [11,18,22], whereas the charge density fluctuations may contribute to a nearly polarization-independent THG signal [22]. In this context, our experimental results appeal for a material-specific theoretical analysis and place a clear constraint on that.

To summarize, the linear and nonlinear response of the superconducting state in the two-band superconductor MgB_2 has been studied by time-resolved terahertz spectroscopy. Third-harmonic generation was observed as a function of temperature for various pump-pulse frequencies. We found resonantly enhanced third-harmonic generation when twice the pump-pulse frequency matches the lower-energy gap $2\Delta_\pi$ that is in the dirty limit (i.e., $\tau^{-1} > 2\Delta_\pi$). In contrast, such resonant behavior is absent for the higher-energy gap of the σ band in the clean limit. Since the THG for an s-wave BCS superconductor in the clean limit should be dominated by charge density fluctuations, our results point to a dominant contribution to the THG from the Higgs amplitude fluctuations in the dirty-limit π band, in agreement with theoretical analyses [14,19]. Nonetheless, complementary pump-probe approaches [46,47] are expected to address further aspects of the nonlinear response of the multiband superconductors, such as the nonlinear response of a clean-limit band, polarization dependence, and effects of interband couplings [4,14–19,48].

Z.W. gratefully acknowledges L. Benfatto, G. Blumberg, I. Eremin, F. Giorgianni, B. B. Jin, I. I. Mazin, R. Shimano, N. Tsuji, and J. Wang for illuminating discussions and/or communications. T.D. acknowledges financial support by the Alexander von Humboldt Foundation. The work in Mainz was partially supported by the

Deutsche Forschungsgemeinschaft (DFG) under Grant No. TRR 173 268565370 (Project A05). The work in Beijing was supported by the National Science Foundation of China (Grant No. 11888101) and the National Key Research and Development Program of China (Grant No. 2017YFA0302904). The work in Cologne was partially supported by the DFG via Project No. 277146847–Collaborative Research Center 1238: Control and Dynamics of Quantum Materials (Subproject No. B05).

S.K. and T.D. contributed equally to this work.

[1] P. W. Anderson, Phys. Rev. **112**, 1900 (1958).
[2] P. W. Anderson, Phys. Rev. **130**, 439 (1963).
[3] D. Pekker and C. M. Varma, Annu. Rev. Condens. Matter Phys. **6**, 269 (2015).
[4] R. Shimano and N. Tsuji, Annu. Rev. Condens. Matter Phys. **11**, 103 (2020).
[5] R. Matsunaga, N. Tsuji, H. Fujita, A. Sugioka, K. Makise, Y. Uzawa, H. Terai, Z. Wang, H. Aoki, and R. Shimano, Science **345**, 1145 (2014).
[6] N. Tsuji and H. Aoki, Phys. Rev. B **92**, 064508 (2015).
[7] R. Matsunaga, N. Tsuji, K. Makise, H. Terai, H. Aoki, and R. Shimano, Phys. Rev. B **96**, 020505(R) (2017).
[8] X. Yang, C. Vaswani, C. Sundahl, M. Mootz, L. Luo, J. H. Kang, I. E. Perakis, C. B. Eom, and J. Wang, Nat. Photonics **13**, 707 (2019).
[9] C. Vaswani, M. Mootz, C. Sundahl, D. H. Mudiyanselage, J. H. Kang, X. Yang, D. Cheng, C. Huang, R. H. J. Kim, Z. Liu, L. Luo, I. E. Perakis, C. B. Eom, and J. Wang, Phys. Rev. Lett. **124**, 207003 (2020).
[10] H. Chu *et al.*, Nat. Commun. **11**, 1793 (2020).
[11] L. Schwarz and D. Manske, Phys. Rev. B **101**, 184519 (2020).
[12] T. Cea, C. Castellani, and L. Benfatto, Phys. Rev. B **93**, 180507(R) (2016).
[13] N. Tsuji, Y. Murakami, and H. Aoki, Phys. Rev. B **94**, 224519 (2016).
[14] R. Haenel, P. Froese, D. Manske, and L. Schwarz, Phys. Rev. B **104**, 134504 (2021).
[15] H. Krull, N. Bittner, G. S. Uhrig, D. Manske, and A. P. Schnyder, Nat. Commun. **7**, 11921 (2016).
[16] T. Cea and L. Benfatto, Phys. Rev. B **94**, 064512 (2016).
[17] Y. Murotani, N. Tsuji, and H. Aoki, Phys. Rev. B **95**, 104503 (2017).
[18] T. Cea, P. Barone, C. Castellani, and L. Benfatto, Phys. Rev. B **97**, 094516 (2018).
[19] Y. Murotani and R. Shimano, Phys. Rev. B **99**, 224510 (2019).
[20] T. Yu and M. W. Wu, Phys. Rev. B **96**, 155311 (2017).
[21] M. Silaev, Phys. Rev. B **99**, 224511 (2019).
[22] G. Seibold, M. Udina, C. Castellani, and L. Benfatto, Phys. Rev. B **103**, 014512 (2021).
[23] C. Zhang, Y. Wang, D. Wang, Y. Zhang, Q. R. Feng, and Z. Z. Gan, IEEE Trans. Appl. Supercond. **23**, 7500204 (2013).
[24] C. Zhang, Y. Wang, D. Wang, Y. Zhang, Z. H. Liu, Q. R. Feng, and Z. Z. Gan, J. Appl. Phys. **114**, 023903 (2013).
[25] C. G. Zhuang, S. Meng, C. Y. Zhang, Q. R. Feng, Z. Z. Gan, H. Yang, Y. Jia, H. H. Wen, and X. X. Xi, J. Appl. Phys. **104**, 013924 (2008).
[26] L. Y. Shi, Y. Q. Liu, T. Lin, M. Y. Zhang, S. J. Zhang, L. Wang, Y. G. Shi, T. Dong, and N. L. Wang, Phys. Rev. B **98**, 094414 (2018).
[27] K.-L. Yeh, M. C. Hoffmann, J. Hebling, and K. A. Nelson, Appl. Phys. Lett. **90**, 171121 (2007).
[28] S. Kovalev, R. M. A. Dantas, S. Germanskiy, J.-C. Deinert, B. Green, I. Ilyakov, N. Awari, M. Chen, M. Bawatna, J. Ling, F. Xiu, P. H. M. van Loosdrecht, P. Surówka, T. Oka, and Z. Wang, Nat. Commun. **11**, 2451 (2020).
[29] J. Nagamatsu, N. Nakagawa, T. Muranaka, Y. Zenitani, and J. Akimitsu, Nature (London) **410**, 63 (2001).
[30] J. Kortus, I. I. Mazin, K. D. Belashchenko, V. P. Antropov, and L. L. Boyer, Phys. Rev. Lett. **86**, 4656 (2001).
[31] M. Iavarone, G. Karapetrov, A. E. Koshelev, W. K. Kwok, G. W. Crabtree, D. G. Hinks, W. N. Kang, E.-M. Choi, H.-J. Kim, H.-J. Kim, and S. I. Lee, Phys. Rev. Lett. **89**, 187002 (2002).
[32] S. Souma, Y. Machida, T. Sato, T. Takahashi, H. Matsui, S. C. Wang, H. Ding, A. Kaminski, J. C. Campuzano, S. Sasaki, and K. Kadowaki, Nature (London) **423**, 65 (2003).
[33] P. C. Canfield and G. W. Crabtree, Phys. Today **56**(3), 34 (2003).
[34] X. X. Xi, Rep. Prog. Phys. **71**, 116501 (2008).
[35] D. Vollhardt, Phys. Rev. Lett. **78**, 1307 (1997).
[36] M. Greger, M. Kollar, and D. Vollhardt, Phys. Rev. B **87**, 195140 (2013).
[37] Z. Wang, M. Schmidt, J. Fischer, V. Tsurkan, M. Greger, D. Vollhardt, A. Loidl, and J. Deisenhofer, Nat. Commun. **5**, 3202 (2014).
[38] R. A. Kaindl, M. A. Carnahan, J. Orenstein, D. S. Chemla, H. M. Christen, H.-Y. Zhai, M. Paranthaman, and D. H. Lowndes, Phys. Rev. Lett. **88**, 027003 (2001).
[39] J. J. Tu, G. L. Carr, V. Perebeinos, C. C. Homes, M. Strongin, P. B. Allen, W. N. Kang, E.-M. Choi, H.-J. Kim, and S.-I. Lee, Phys. Rev. Lett. **87**, 277001 (2001).
[40] B. B. Jin, P. Kuzel, F. Kadlec, T. Dahm, J. M. Redwing, A. V. Pogrebnyakov, X. X. Xi, and N. Klein, Appl. Phys. Lett. **87**, 092503 (2005).
[41] A. V. Pronin, A. Pimenov, A. Loidl, and S. I. Krasnosvobodtsev, Phys. Rev. Lett. **87**, 097003 (2001).
[42] V. Guritanu, A. B. Kuzmenko, D. van der Marel, S. M. Kazakov, N. D. Zhigadlo, and J. Karpinski, Phys. Rev. B **73**, 104509 (2006).
[43] M. Ortolani, P. Dore, D. Di Castro, A. Perucchi, S. Lupi, V. Ferrando, M. Putti, I. Pallecchi, C. Ferdeghini, and X. X. Xi, Phys. Rev. B **77**, 100507(R) (2008).
[44] G. Blumberg, A. Mialitsin, B. S. Dennis, M. V. Klein, N. D. Zhigadlo, and J. Karpinski, Phys. Rev. Lett. **99**, 227002 (2007).
[45] G. Blumberg, A. Mialitsin, B. S. Dennis, N. D. Zhigadlo, and J. Karpinski, Physica C **46**, 75 (2007).
[46] F. Giorgianni, T. Cea, C. Vicario, C. P. Hauri, W. K. Withanage, X. Xi, and L. Benfatto, Nat. Phys. **15**, 341 (2019).
[47] K. Katsumi, N. Tsuji, Y. I. Hamada, R. Matsunaga, J. Schneeloch, R. D. Zhong, G. D. Gu, H. Aoki, Y. Gallais, and R. Shimano, Phys. Rev. Lett. **120**, 117001 (2018).
[48] M. A. Müller and I. M. Eremin, arXiv:2107.02834.